



Effective green ammonia synthesis from gaseous nitrogen and CO₂ saturated-water vapour utilizing a novel photocatalytic reactor

A.W. Morawski^a, K. Ćmielewska^a, E. Ekiert^{a,*}, E. Kusiak-Nejman^a, I. Pelech^a, P. Staciwa^a, D. Sibera^{a,b}, A. Wanag^a, J. Kapica-Kozar^a, M. Gano^c, Z. Lendzion-Bieluń^a, U. Narkiewicz^a

^a Department of Inorganic Chemical Technology and Environment Engineering, Faculty of Chemical Technology and Engineering, West Pomeranian University of Technology in Szczecin, Pulaskiego 10, 70-322 Szczecin, Poland

^b Department of General Civil Engineering, Faculty of Civil and Environmental Engineering, West Pomeranian University of Technology in Szczecin, Piastow 50 a, 70-311 Szczecin, Poland

^c Department of Organic Chemical Technology and Polymer Materials, Faculty of Chemical Technology and Engineering, West Pomeranian University of Technology in Szczecin, Pulaskiego 10, 70-322 Szczecin, Poland

ARTICLE INFO

Keywords:

Photocatalysis
New photocatalytic reactor
Nitrogen fixation
Green ammonia

ABSTRACT

The ammonia synthesis from nitrogen and hydrogen derived from water vapor in the photocatalytic process performed under mild conditions is presented. A new solution of a gas-phase photocatalytic reactor with the bed in the form of a UV transparent glass fiber cloth coated with AEROXIDE® P25 TiO₂ was applied. The bed in the reactor is located just above the water surface. The gases circulate from above towards the water surface, where the produced ammonia is easily absorbed and continuously separated from the gas phase, shifting the ammonia synthesis equilibrium towards the product. The highest amount of ammonia (about 1.3 mmol NH₄⁺/g TiO₂ after 6 h) was obtained at 20 °C, and with the use of the gaseous mixture containing CO₂ (15%), N₂ (85%), and water vapour derived from water located at the bottom of the reactor. Carbon dioxide in the reaction environment is simultaneously reduced to carbon monoxide and methane.

1. Introduction

Producing ammonia from nitrogen and hydrogen gas by the Haber-Bosch method at an industrial scale is an expensive process. Due to kinetic reasons, it requires high pressure of 15–30 MPa [1] and high temperatures at 400–600 °C [2]. This, in turn, translates into CO₂ emissions to the atmosphere. An additional carbon dioxide emission source is the hydrogen preparation stage for ammonia synthesis, where methane-steam conversion is used, followed by the separation of CO₂ from post-conversion gases. Therefore, the Haber-Bosch method is associated with high energy consumption at the level of 1–2% of total world energy consumption and accounts for 1.44% of CO₂ global emissions [3].

For several decades, work on an attractive attempt to convert nitrogen to ammonia using the photocatalytic method has been underway. This procedure assumes the application of photoactive semiconductors, mainly titanium dioxide and water. In this method, under atmospheric pressure and ambient temperature, water is a source of hydrogen for the synthesis of so-called green ammonia from nitrogen.

The reaction of synthesizing an ammonia molecule is exothermic, so running the process at low temperatures favorably shifts the equilibrium towards product formation. An ongoing challenge is finding photocatalytic solutions that result in higher kinetics under mild conditions.

Contrary to the energy-demanding Haber-Bosch process, the photocatalytic reduction is an environmentally friendly solution for ammonia production, which can be performed under mild conditions. Another advantage of this solution is that light energy can be applied, and water can be used as a reducing agent. The photocatalytic reduction mechanism using semiconductors consists of water oxidation by photoenergy-formed valence band holes and reduction of N₂ by conduction band electrons. Consequently, ammonia is produced from water and N₂ under mild conditions [4].

Among all the well-known photocatalysts, TiO₂ is the most prominent material and has been applied in photocatalytic applications because of its abundance, efficient charge separation and stability [5,6]. Moreover, a recently strong effort has been applied to enhance the photocatalytic activity of TiO₂ even more through doping with nitrogen [7], carbon [8] or noble metals [9].

* Corresponding author.

E-mail address: edabrowa@zut.edu.pl (E. Ekiert).

<https://doi.org/10.1016/j.cej.2022.137030>

The first publication concerning the reduction of nitrogen in water to ammonia using TiO₂ was described by Schrauzer and Guth [10]. The authors obtained the highest amounts of produced ammonia using rutile/anatase photocatalyst (95/5) modified with 0.2% Fe₂O₃ during 4 h of irradiation with a 360 W Hg-Arc lamp. In a process performed at 40 °C, using 0.2 g of the photocatalyst, 6.6 μmol of ammonia (NH₃) and 0.14 μmol of hydrazine (N₂H₄) were obtained. Other facts observed by the authors were the effects of nitrogen adsorption and temperature on performance. It was shown that increasing the N₂ pressure from 0.3 atm to 1.5 atm increases the yield of ammonia from 1.53 μmol to 6.95 μmol. On the other hand, an increase in temperature from 30 to 50 °C increases the efficiency, respectively, from 4.8 μmol to 6.0 μmol after 3 h of irradiation. Above 50 °C, a significant reduction in the yield of the reaction was observed. In summarizing these results, presented later by Schrauzer [11], the photocatalytic nitrogen reduction mechanism was suggested, which showed that hydrazine was an intermediate product in the formation of ammonia.

In recent years, there has been a significant increase in interest in photocatalytic methods of nitrogen fixation on TiO₂ photocatalysts. One of the methods of increasing the efficiency of nitrogen binding to ammonia was an attempt to produce titanium dioxide nanotubes with gold depositing on them [12]. The best photocatalyst with 3 wt% of Au produced about 5.5 μmol/l of ammonia during 5 h of the reaction. Additionally, the activity slightly decreased with subsequent repetition cycles. Au anchoring on TiO₂ generally improves nitrogen adsorption capacity, promotes the formation of oxygen vacancies, and enhances charge separation, resulting in higher ammonia formation using the photocatalyst. Li et al. [13] synthesized N-doping TiO₂ hollow microspheres with oxygen vacancies that are crucial for improving photoactivity because of light absorption and photocarriers' separation. The ammonia yield formation achieves 80.09 μmol/g/h under a 300 W Xenon lamp, synergizing effects between the oxygen vacancies and the hollow microspheres. Increased efficiency of ammonia formation to 183.02 μmol/g/h was achieved on samples in which molybdenum was introduced into mesoporous TiO₂ [14]. The use of computational methods has shown that a single Fe atom loaded on anatase TiO₂ (001) can promote electron-hole separation and enhance the nitrogen fixation to ammonia. Also, nitrogen photofixation on Fe-doped TiO₂ with highly exposed (101) facets was experimentally confirmed [15]. Theoretical calculations also show that on the rutile form of TiO₂ (110), it is possible to fixate nitrogen in water to ammonia [16,17]. The rutile form of TiO₂ with oxygen vacancies for the production of ammonia has been shown in the paper [18]. Using the Xe lamp for irradiation, the efficiency of 116 μmol/g/h was achieved. The work results in which ruthenium was used as a TiO₂ admixture showed that the highest activity was 56.3 μmol/g/h [19,20].

Some publications for photocatalytic fixation of nitrogen are shown in Table 1.

The photocatalytic method has several additional disadvantages concerning fixing nitrogen to ammonia. These include still low reaction yields and the need to separate TiO₂ from the aqueous suspension. Recently, there has been experimental evidence that the ammonia synthesis reaction on TiO₂ is inhibited by secondary ammonia oxidation [11].

This paper presents a novel and groundbreaking method of avoiding the mentioned disadvantages, e.g. separating the photocatalyst from the water suspension by immobilizing TiO₂ on a UV-transparent quartz cloth and placing it just above the water surface, which prevents the secondary oxidation of the produced ammonia through its rapid absorption in water. Unexpectedly, it turned out that such a solution led to the production of ammonia with yields many times higher than the data in the previously cited literature related to the photocatalytic fixation of nitrogen to ammonia. Placing the quartz fabric with immobilized TiO₂ just above the water surface is crucial, as it enables higher nitrogen adsorption from the gas phase, which is decisive for the ammonia synthesis reaction [11,12,28,29], and rapid absorption of gaseous ammonia

Table 1
Details of papers concerning photocatalytic nitrogen fixation.

Photocatalysts	Mass	Liquid phase	Light source	Yield	Reference
PAN/BiOBr-Cl microfibers	–	deionized water	300 W Xe lamp	234.4 μmol/g/h	[21]
La/MoO _{3-x}	20 mg	deionized water	300 W Xe lamp	209 μmol/g/h	[22]
TiO ₂ /BiOBr 2D-2D	25 mg	10 vol% MeOH aqueous solution	300 W Xe lamp	1.43 mmol/g/h	[23]
Microcystis@TiO ₂	20 mg	10 vol% MeOH aqueous solution	300 W Xe lamp	0.97 mmol/g/h	[24]
TPA@CoFe ₂ O ₄	30 mg	Na ₂ SO ₃ aqueous solution	500 W solar lamp	215 μmol/h	[25]
g-C ₃ N ₄ /CeFeO ₃	–	–	UV-A LED	573.1 μmol/l/g	[26]
N-doped TiO ₂	20 mg	deionized water	300 W Xe lamp	80.1 μmol/g/h	[13]
Mo-doped TiO ₂	100 mg	deionized water	300 W Xe lamp	183 μmol/g/h	[14]
Ru-decorated TiO ₂	40 mg	20 vol% EtOH aqueous solution	300 W Xe lamp	56.3 μg/g/h	[19]
Ru/TiO ₂ (P25)	50 mg	ultrapure water	300 W Xe lamp	419 μmol/l/g	[20]
AgPt/TiO ₂	5 mg	ultrapure water	300 W Xe lamp	38.4 μmol/g/h	[27]

in water to NH₄⁺ ions, which shifts the reaction equilibrium towards the product. The major limitations of gas–liquid processes with suspended photocatalyst nanoparticles in solution could be defined as low stability in gaseous nitrogen in water (it is more efficient to conduct the N₂ fixation process in a gas phase), competitiveness of hydrogen evolution reaction, and above-mentioned secondary ammonia oxidation mainly by photogenerated holes, as well as other reactive oxygen species [30]. By conducting the ammonia photoreduction process in the gas phase, we limit the negative effects of certain phenomena occurring when conducting the process in the aqueous phase.

In addition, the use of a glass fiber carrier should be advantageous, as it has been described in the literature that silica in various crystallinity and morphology forms -foams, spherical [31–34]- increases the photocatalytic activity by interacting with the functional groups of TiO₂, including Ti–O–Si chemical bond formation [34].

In this work, we took up a new challenge to carry out the photofixation reaction of gaseous nitrogen with water vapor saturated with carbon dioxide.

2. Experimental

2.1. Photocatalyst-coated glass fiber preparation and characterization

In the experiments, photocatalysts consisting of AEROXIDE® TiO₂ P25 type manufactured by Evonik Industries AG (previously Degussa, Germany) were tested in various gaseous reactions and temperatures. The pure TiO₂ (S_{BET} = 54 m²/g; 89% of anatase with crystallite size of 27 nm, and 11% of rutile with crystallite size of 43 nm) was applied on the glass fiber cloth with the density of 40 g/m², supplied by Fiberglass Fabrics (Poland). A detailed characterization of the P25 used in the

study can be found elsewhere [35,36]. In order to put the photocatalyst on the support, four strips of the glass fiber fabric with dimensions of $4 \times 8 \times 0.25$ cm were weighed. Then, 0.5 g of TiO_2 was weighed out and mixed with 4 cm^3 of 96% ethanol and 3 cm^3 of distilled water. Finally, the mixture was applied by spraying the strips of glass fiber cloth. The prepared material was dried in an oven at $110 \text{ }^\circ\text{C}$ for 30 min. The cloth was weighed after drying to determine the weight of the deposited photocatalyst.

The surface morphology of the samples was investigated with a scanning electron microscope (SEM Hitachi SU 8020, Japan). The analysis parameters were: acceleration voltage of 5 kV for SEM, 20 kV for EDX, current of $10 \mu\text{A}$ for both techniques.

The samples for investigation with SEM were firstly evaporated with a 5 nm of chromium, which thin layer prevented samples from electric charging.

AFM pictures were taken with an AFM NanoScope V Multimode 8 microscope (Bruker Corporation, United States). Measurements were made with a ScanAsyst-Air silicon nitride probe in ScanAsyst, using contact mode. The scan area was $5 \times 5 \mu\text{m}$.

TG-DTG analysis was conducted using NETZSCH STA 449 F3 Jupiter (Erich NETZSCH GmbH & Co. Holding KG, Germany) equipped with a silicon carbide SiC oven and S-type TG/DTA thermocouple. The measurements were carried out at a temperature of $30 - 1000 \text{ }^\circ\text{C}$ and samples mass of about 10 mg. Samples were heated in an open Al_2O_3 crucible with a corresponding empty referent pan at a heating rate of $10 \text{ }^\circ\text{C}/\text{min}$, using argon as a chemically inert gas ($70 \text{ ml}/\text{min}$). Additionally, the measurements were also carried out in the oxidative atmosphere using air ($60 \text{ ml}/\text{min}$) and protective argon ($10 \text{ ml}/\text{min}$) mixture.

2.2. Reactor system

The experiments were carried out in a cylindrical quartz reactor with a working capacity of 392 cm^3 , located in a thermostatic chamber. A diagram illustrating the operation is shown in Fig. 1a. Moreover, Fig. 1b shows a picture of a quartz glass reactor prepared for the gas-phase process. The beds consisting of quartz fibers covered with TiO_2 can be seen inside the reactor. Four Actinic BL TL-E Philips lamps with a total power of 88 W were used for irradiation, emitting UV-A radiation in the

wavelength range of 350–400 nm. The radiation spectrum of lamps was presented in Fig. 2 [37]. The lamps were placed outside the reactor, forming a set of four rings. The reactor was closed in a thermostatic chamber to cut off other light sources and ensure a stable process temperature. Next, 3 cm^3 of distilled water was poured into the reactor. Next, a photocatalyst, previously immobilized on glass fiber (0.63 g glass fiber cloth and 0.26 g TiO_2), was inserted into the reactor. Then, a whole system was rinsed with pure nitrogen (99.999%); or the mixture of nitrogen (85%) with CO_2 (15%); or the mixture of CO_2 (97%) with air (2.5%-1.975% N_2 and 0.525% O_2), supplied by (Messer, Poland) for 30 min. After this time, the system was tightly closed, and the lamps were turned on. During the rinsing gas was stirred using the pump with a flow rate equal to $1.6 \text{ dm}^3/\text{h}$. The process was carried out for 6 h. Three experiments were performed at $20 \text{ }^\circ\text{C}$, and one activity measurement was conducted at $50 \text{ }^\circ\text{C}$. For the temperature of $20 \text{ }^\circ\text{C}$, the pressure of water steam saturation was 2.3 kPa, and for the temperature of $50 \text{ }^\circ\text{C}$, this pressure was 12.3 kPa.

2.3. Photocatalysis products analysis

After the process, the reactor was opened, and water was collected to determine the value of pH and the content of ammonia (NH_4^+ ions). The sensitive and economical Nessler method used the UV-Vis spectrophotometer V-650 (JASCO International Co., Japan) for the analysis, which

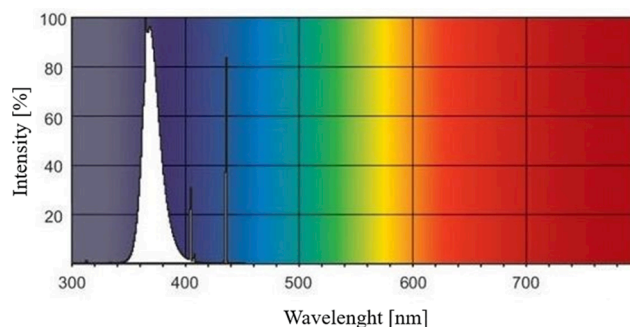


Fig. 2. The light spectrum of used Actinic BL TL-E Philips lamps [37].

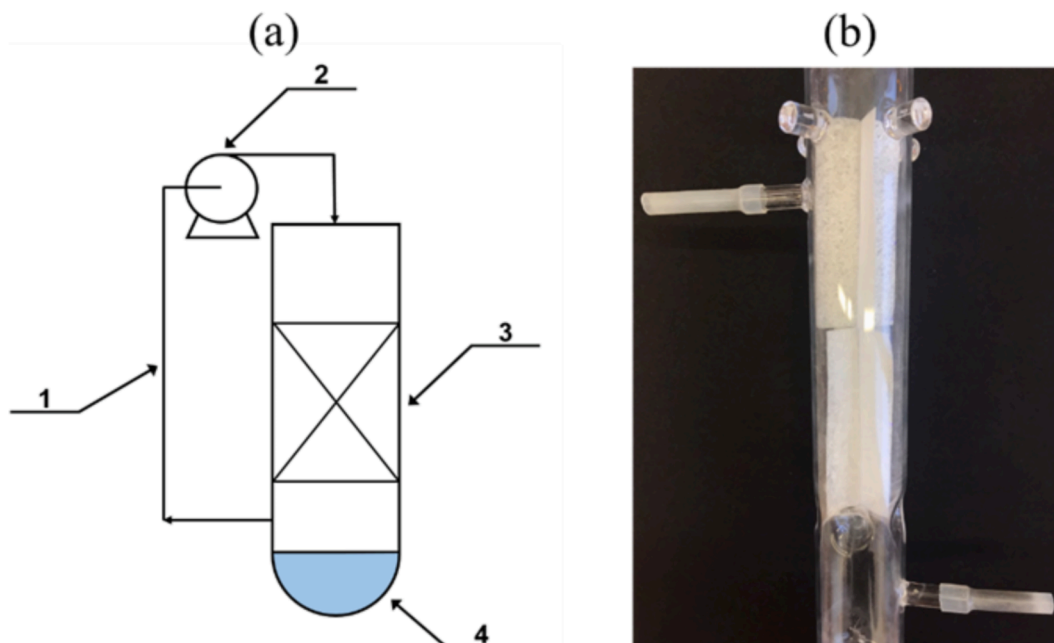


Fig. 1. The scheme of the reactor (a): 1 – gas circulation loop; 2 – pump; 3 – photocatalyst on a glass fiber cloth; 4 – water; quartz reactor with a bed made out of photocatalyst applied on glass fiber cloth (b).

can also be applied for this purpose [38].

The gas-phase composition was analyzed using the SRI 310C gas chromatograph (SRI Instruments, USA), equipped with a 5Å molecular sieve column and an HID detector (Helium Ionization Detector). The carrier gas was helium. The analyzes were carried out under isothermal conditions at 60 °C. The gas flow through the column was 60 cm³/min, while the volume of the tested gas sample was 1 cm³. The content of individual components in the gas phase in subsequent measurements was calculated based on the calibration curve.

3. Results and discussion

3.1. Photocatalyst-coated glass fibres characterization

SEM images and the surface composition determined by the EDX method of a pure silica cloth were presented in an earlier publication [39]. The surface morphology of pure glass fiber fabric and coated with P25 TiO₂ are presented in Fig. 3a and 3b, respectively. It can be seen that a single fiber diameter varies in the range from 15 to 30 μm. Fibers can also form multi-fiber structures, shown in Fig. 3c. Titanium dioxide forms clusters of various sizes which totally cover the fibers surface and create aggregates in spaces between glass fibers what is typical for the used method of active phase deposition [40]. Measurements in the form of a map of the distribution of elements made using the EDX technique are shown in Fig. 3d. Standard EDX spectrum obtained for P25-coated glass fibres is shown in Fig. 4, based on which the chemical surface composition was calculated and shown in Table 2. Silicon, aluminum, calcium, and some oxygen come from the glass fibers, while titanium and oxygen come from the deposited titanium dioxide. The titanium content on the surface is close to 17 wt% (ca. 10 at%), as shown in

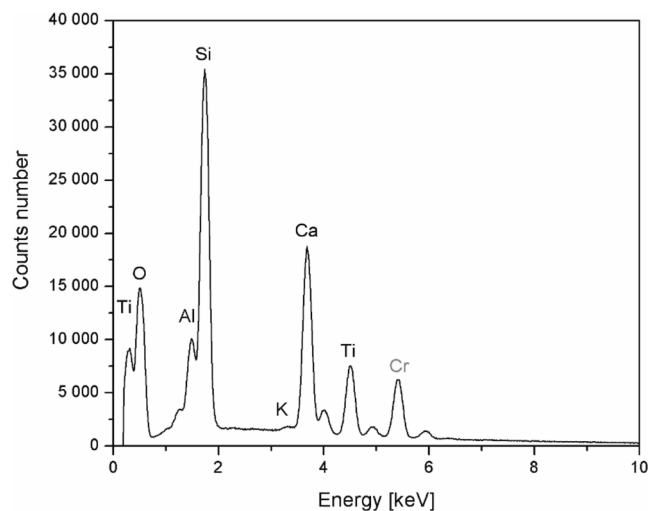


Fig. 4. EDX spectrum of P25-coated glass fibres.

Table 2. Chromium seen in the EDX spectrum comes from the stage of sample preparation stage for SEM imaging – thin layer of chromium prevents electron charging of sample during the SEM analysis. Chromium was excluded for calculation of sample chemical surface composition.

The scan images taken with the AFM technique are presented in Fig. 5. Fig. 5a shows the surface of clean glass fibers with a visible curvature of the fiber surface before being covered with a photocatalyst. On the other hand, Fig. 5b confirms the deposition of TiO₂ on the oval

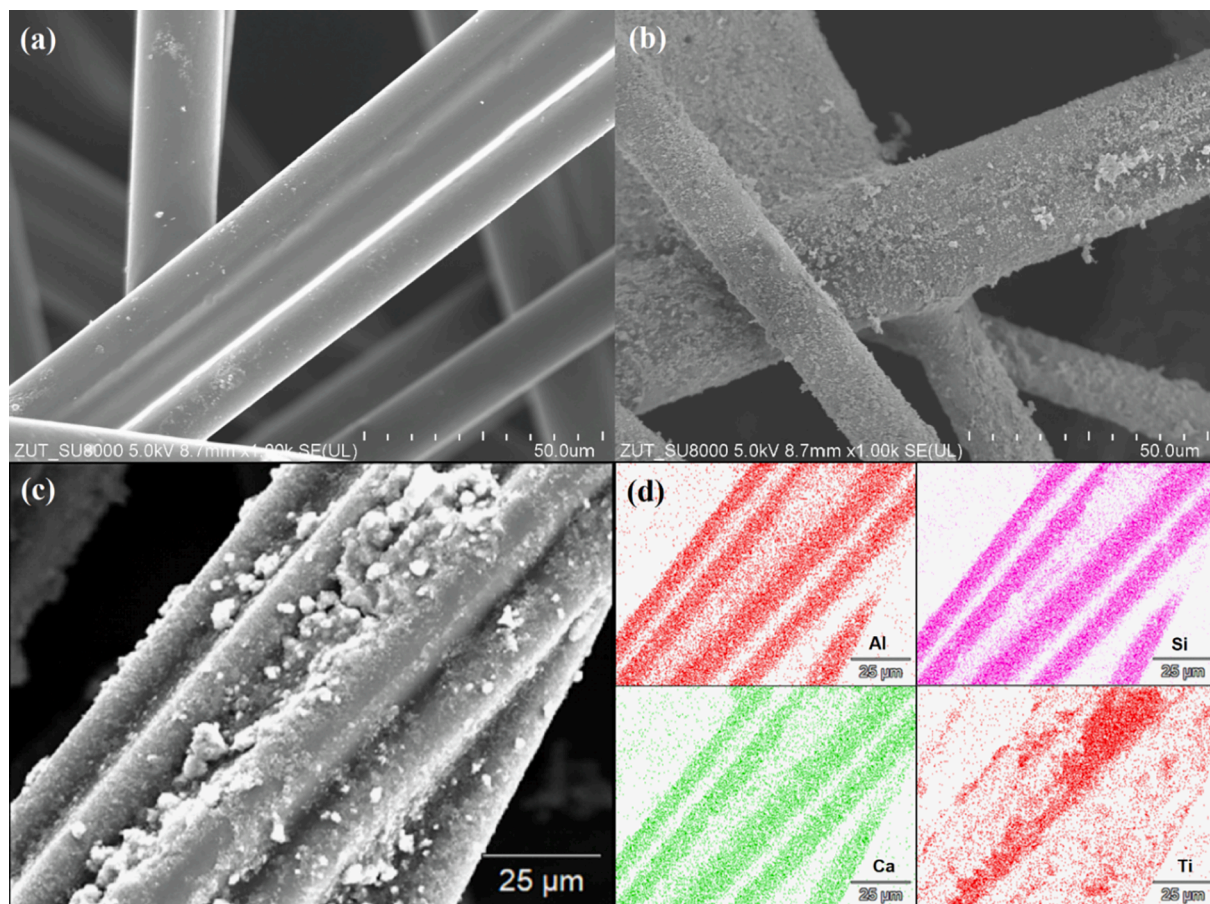


Fig. 3. SEM images of pure glass fibres (a) and P25-coated glass fibres (b, c) and EDX chemical elements mapping (d) of area shown in (c).

Table 2
Chemical surface composition of glass fiber fabric coated with P25 TiO₂.

Element line	Intensity [cps/nA]	wt%	at%
O K	151.709	15.3	27.7
Al K	697.067	5.4	5.8
Si K	4687.61	34.9	36.2
K K	41.563	0.4	0.3
Ca K	2843.15	27.2	19.8
Ti K	1149.52	16.8	10.2
Total		100.00	100.00

surface of a single non-woven fabric. It can be observed that TiO₂ occurs in the form of very small, single particles or clusters. The surface of the fiber is well covered by the photocatalyst.

Fig. 6a,b and 7a,b show the results of the TG/DTG analysis of the investigated samples. The TG-DTG curves consist of four steps for the thermal decomposition process and exhibit a very similar character. The first one starts at the temperature range of 30–C, corresponding to the differential thermogravimetric (DTG) profile, with the maximum temperature at 80 °C corresponding to the elimination of physically retained water. At the temperature range above 250 °C, we observed a second step between 180 and 360 °C, reaching a weight loss of 12.4 %, 4.4 % and 7.2 % in an inert atmosphere and 11.5 %, 8.8 %, 7.3 % in an oxidative atmosphere for pure glass fiber, glass fiber coated with P25 and glass fiber coated with P25 after of the photocatalytic reaction, reaching a maximum rate of decomposition (DTG profile) at 287 °C, 285 °C and 263 °C, respectively which corresponds to the dehydration of calcium silicate hydrates [41]. Finally, the third peak at the temperature range of 360–450 °C, reaching the maximum rate of decomposition at 390 °C (DTG curves) and comprising roughly 4.1 %, 1.5 % and 2.2 % of the total mass loss (TG curves) for pure glass fiber and glass fiber coated with P25 before and after photocatalytic reaction (Fig. 6a,b), correspond to the formation aluminium oxyhydroxide compound [42]. In the case of the samples clothed with TiO₂ P25, we observe four steps at the temperature range of 650–880 °C, reaching the maximum at 820 °C and characterized by a negligible mass loss (of 1.6 % and 1.1 %) for the glass fiber coated with P25 before and after photocatalytic reaction which can be correlated with the transforms of anatase-to-rutile [42].

In the case of the DTG measured in an oxidizing atmosphere (Fig. 7a, b), we can observe the difference in the weight losses and also different maximum rates of decomposition compared with the DTG curves measured in an inert atmosphere in the case of the third step at the temperature range 360–450 °C (Fig. 6a,b). The maximum decomposition rate is shifted towards lower values, reaching the maximum value at 350 °C, comprising roughly 4.4 %, 3.2 %, and 2.7 % of the total mass loss (TG curves). Moreover, in the air atmosphere, we can observe additional weight loss in the temperature range of 400–630 °C and reach the mass loss of ca. 2.5 % for all the materials, accompanied by the complete decomposition of aluminum oxyhydroxide compound to aluminum oxide [43].

3.2. Performance of the photocatalytic process

Table 3 presents the results of measurements of the nitrogen fixation activity towards the formation of ammonia, which was absorbed in the water under the photocatalytic bed according to the following 6-electron overall reaction (1) [44]:



The reaction products were determined as NH₄⁺ ions. It can be seen that with the formation of ammonia, the pH of the water increased depending on the composition of the starting gas used. For the sample P25 (CO₂ + air), highly saturated with CO₂ (97.5%), the pH increased from approx. 5 to 7. For the samples with lower CO₂ content, an increase from 6–7 to about 8–9 was observed. However, in the case of the P25 (N₂) sample with pure nitrogen, the pH increased from neutral to approx. 8.

In the beginning, preliminary experiments were carried out due to eliminating the effect of photolysis or the photoactivity of the material used as a matrix for applied photocatalyst. Results concerning those tests are presented in Table 3. Photolysis 1 and Photolysis 2 were conducted without any photocatalyst or silica cloth, only with water, and with two different gases (CO₂ + air, and the mixture of CO₂ and N₂, respectively). The experiment marked as Blank (pure silica cloth) was carried out in a mixture of CO₂ and N₂. In this case, except water, the pure glass fiber was also placed in the reactor. No measurable amounts of photoreduction products were observed in these processes, both in the liquid and gas phases.

As shown in Table 3, 0.6 mmol NH₄⁺ was produced per 1 g of TiO₂ after 6 h with a low nitrogen content (1.975%), oxygen, and CO₂ in the reaction gases for the sample P25 (CO₂ + air). Removal of oxygen and increasing the amount of nitrogen in the mixture to 85% with CO₂ (sample P25 (CO₂ + N₂)) resulted in a twofold increase in the concentration of NH₄⁺ ions in water to 1.28 mmol NH₄⁺/g TiO₂ after 6 h. The temperature has little influence on nitrogen fixation. However, raising the temperature from 20 to 50 °C increased the ammonium ion concentration to 1.34 mmol NH₄⁺/g TiO₂ (sample P25 (CO₂ + N₂ 50 °C)). Moreover, the introduction of very pure nitrogen to the photoreactor (99.999% N₂ for the (P25 N₂) sample) did not cause a significant increase, but even a decrease in the amount of NH₄⁺ ion produced was observed (1.1 mmol NH₄⁺/g TiO₂).

Inside the photoreactor, there is a carbonate equilibrium between the gaseous CO₂ and water (except for the P25 (N₂) sample without any CO₂), which can be represented by the following reactions (2)–(5) [45]:

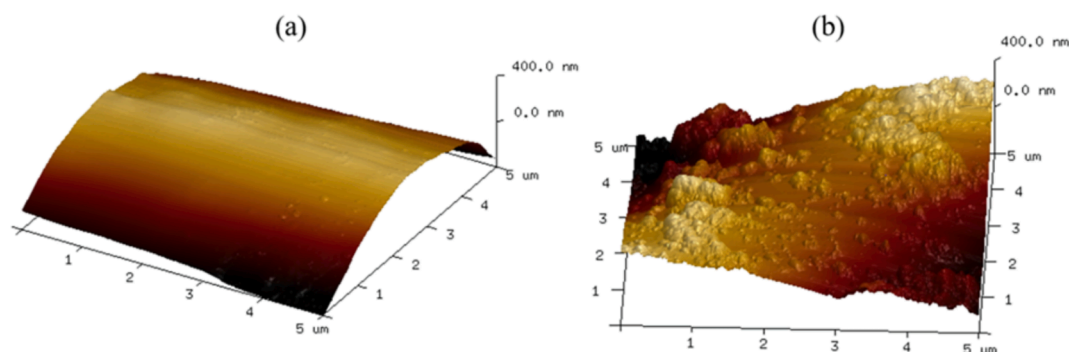
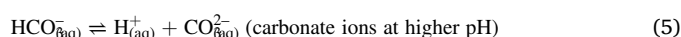
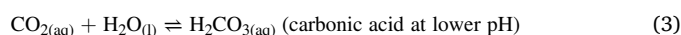


Fig. 5. AFM scan images of pure glass fiber fabric (a) and glass fiber fabrics with P25 TiO₂ on a single fiber (b).

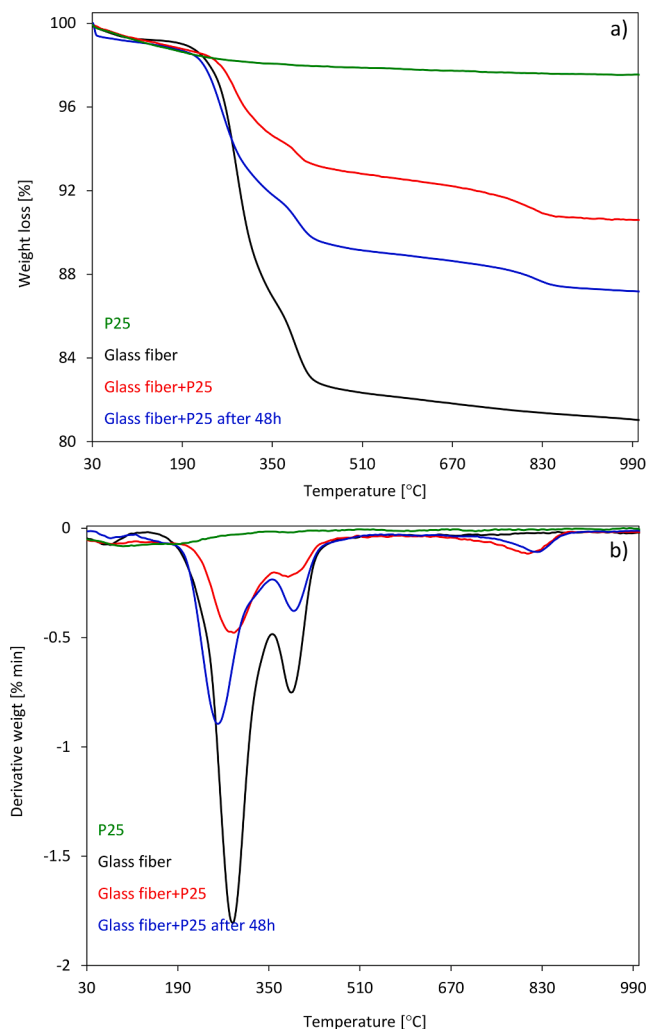


Fig. 6. Thermogravimetric weight loss process of reference P25 and tested hybrid composites: TG (a) and DTG (b) measured in an inert atmosphere.

The equilibrium between CO_2 in the gas phase and CO_2 dissolved in water proposed in the above reactions (2)-(5) at constant pressure depends on the pH and temperature. At the beginning of the photocatalytic reaction at a temperature of 20°C for nitrogen fixation, pH equals 5 for high CO_2 concentration (97.5%), through pH equals 6 for lower CO_2 concentration (15%). Increasing the reaction temperature to 50°C increased the pH to 7 due to a higher level of CO_2 desorption compared to 20°C .

As a result of the equilibrium conditions described in reactions (2)-(5), the produced ammonia reacts immediately in water, and in the pH range between 7 and 9, it mainly forms ammonium bicarbonate NH_4HCO_3 . In this range, bicarbonate ions dominate with participation in carbonate equilibrium from 80% to 95.7% [46]. However, for a pH above 7.4, carbonate ions appear gradually, and small amounts of ammonium carbonate $(\text{NH}_4)_2\text{CO}_3$ may also be present - up to a maximum of 4% at pH equals 9.

In the summary of the conditions prevailing during the experiments in the photocatalytic reactor with the photocatalyst located above the water surface and at various CO_2 concentrations, it can be stated that the produced ammonia is absorbed in water and reacts to ammonium hydrogen carbonate NH_4HCO_3 or ammonium carbonate $(\text{NH}_4)_2\text{CO}_3$, except for the experiment with the use of P25 (N_2) sample where it appears as NH_4OH .

Additionally, CO_2 absorbed in water easily reacts with photo-generated ammonia dissolved in water according to the following

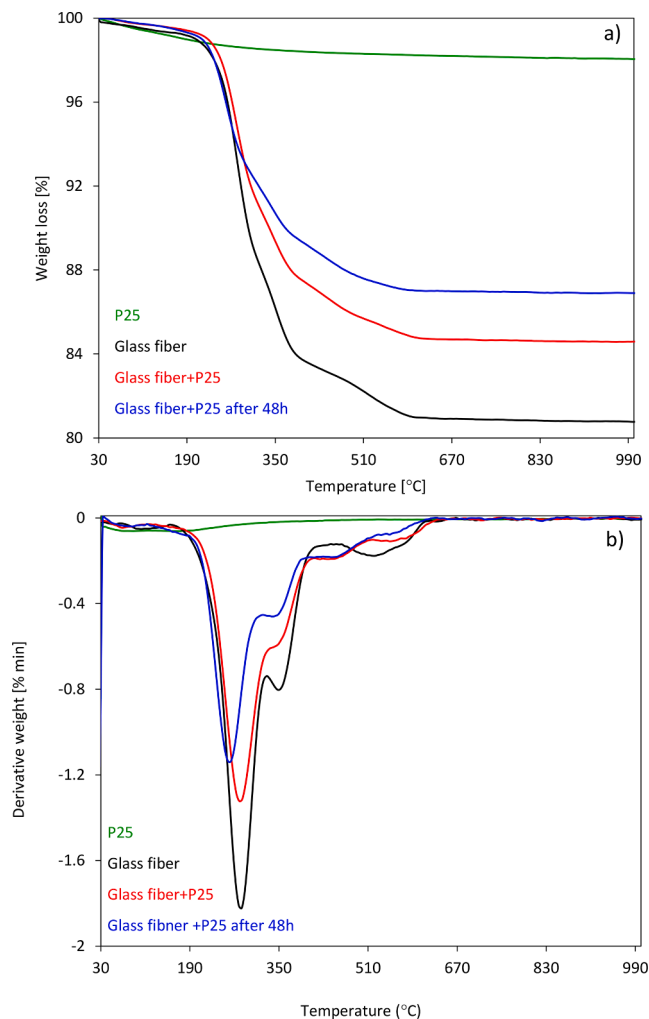


Fig. 7. Thermogravimetric weight loss process of reference P25 and tested hybrid composites: TG (a) and DTG (b) curves measured in an oxidative atmosphere.

reaction (6) [47]:



Ammonium carbamate easily hydrolyzes in solution having an irreversible reaction (7):



The hydrolysis of ammonium carbamate produces additional ammonia molecules, hence the higher amount in our experiment when using a mixture of CO_2 and N_2 as the feed gas. This is also why we observe an increase in pH (see Table 3).

At the same time, some other complex reactions (8) - (9) occur in the solution [48]:



By running the reaction in nitrogen as a feed gas, we eliminate the additional binding agent for the ammonia produced. Therefore, in the case of a process conducted only in the presence of nitrogen, the amount of ammonia generated is lower, and only its absorption in water occurs.

During nitrogen fixation to ammonia, the content of hydrogen (Fig. 8), carbon monoxide (Fig. 9), and methane (Fig. 10) in the gas phase were analyzed simultaneously.

Table 3
Results of photocatalytic ammonia production.

Sample name	Gas phase composition	Temperature, [°C]	Water pH		Production after 6 h	
			before reaction	after reaction	[mg NH ₄ ⁺ /gTiO ₂]	[mmol NH ₄ ⁺ /gTiO ₂]
P25 (CO ₂ + air)	CO ₂ (97.5%), air (2.5%)	20	5	7	10.58	0.60
P25 (CO ₂ + N ₂)	CO ₂ (15%), N ₂ (85%)	20	6	8	23.15	1.28
P25 (CO ₂ + N ₂ 50 °C)	CO ₂ (15%), N ₂ (85%)	50	7	9	24.05	1.34
P25 (N ₂)	N ₂ (99.999%)	20	7	8	19.71	1.10
Photolysis 1	CO ₂ (97.5%), air (2.5%)	20	5	5	method error limit	
Photolysis 2	CO ₂ (15%), N ₂ (85%)	20	6	6	method error limit	
Blank (pure silica cloth)	CO ₂ (15%), N ₂ (85%)	20	6	6	method error limit	

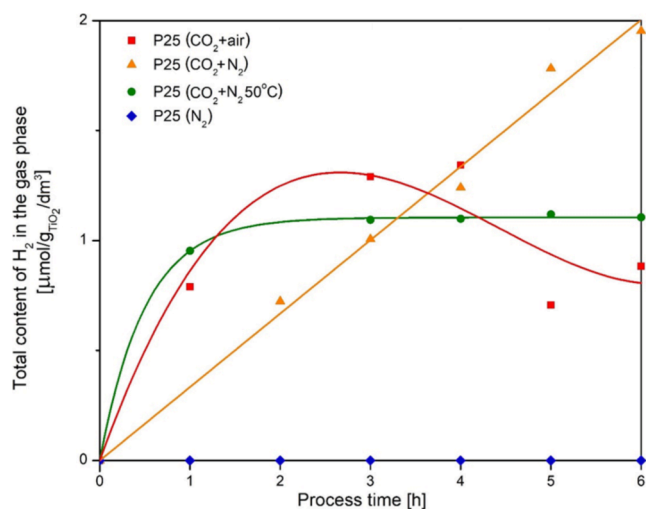


Fig. 8. Hydrogen production in 6 h of the gas process.

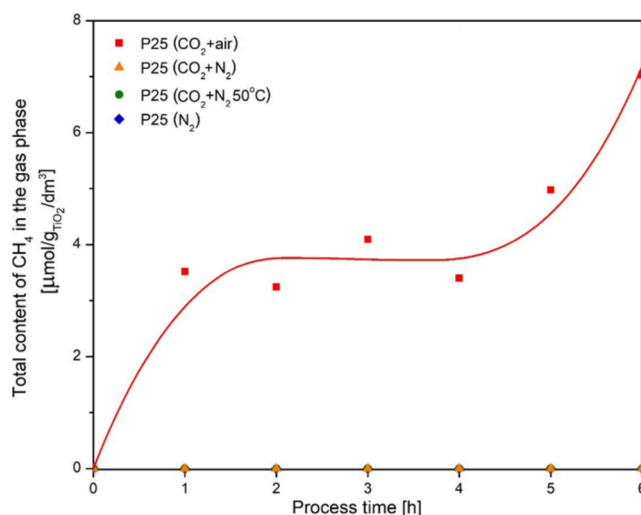


Fig. 10. Methane production in 6 h of the gas process.

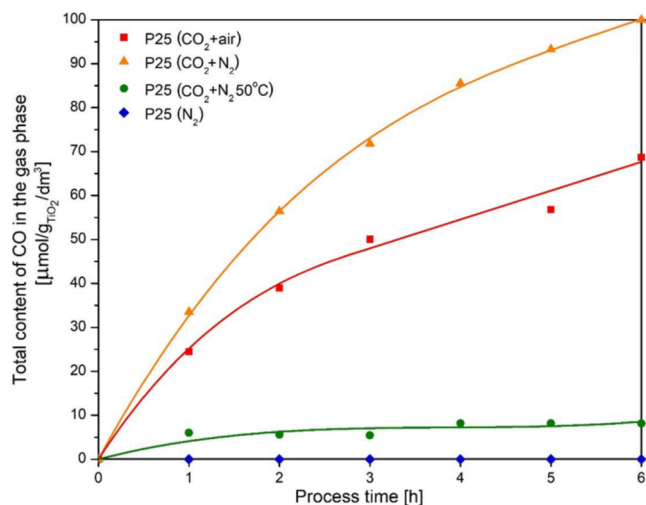


Fig. 9. Carbon monoxide production in 6 h of the gas process.

Fig. 8 shows the changes in hydrogen content as a product of water decomposition. It can be seen that when testing the P25 (CO₂ + N₂) sample at 20 °C, the hydrogen content increases linearly with time to about 2 μmol/g TiO₂/dm³. On the other hand, for samples P25 (CO₂ + N₂ 50 °C) and P25 (CO₂ + air), a level of about 1 was maintained during the measurement. Contrary to the experiments mentioned above, in the experiment with very pure nitrogen 99.999% (sample marked as P25 (N₂)), no hydrogen was detected for 6 h of the measurement.

Fig. 9 shows the carbon monoxide content during 6 h of measurements for various experiments. Carbon monoxide is the product of the reduction of carbon dioxide with hydrogen in a two-electron reaction

[49,50]:



It can be seen that the highest amount of CO was obtained for the experiment P25 (CO₂ + N₂) at the temperature of 20 °C. The carbon monoxide content increased to about 100 μmol/g TiO₂/dm³ after 6 h. A similar course of carbon oxide production is observed for the P25 (CO₂ + air) experiment, with slightly lower production of up to about 60 μmol/g TiO₂/dm³. Increasing the photoreaction temperature resulted in a radical decrease of CO₂ reduction to CO. Only about 5 μmol/g TiO₂/dm³ after 6 h was measured. Obviously, no carbon monoxide was found for studies carried out in the pure nitrogen atmosphere (P25 (N₂) sample).

Fig. 10 shows the formation of methane during the conducted experiments. The formation of methane is a reaction (11) that requires 8 electrons [50,51]:

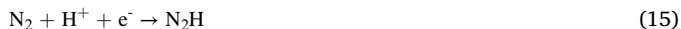
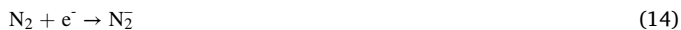


A reaction presented above is more difficult to carry out under these conditions. Only in the case of the experiment performed using P25 (CO₂ + air) a small amount of methane was observed. Its content gradually and unsystematically increased to about 7 μmol/g TiO₂/dm³ after 6 h. In the remaining three experiments, no methane was found in the gas phase after 6 h of the photocatalytic reaction.

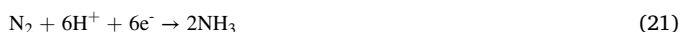
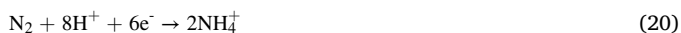
On the homogeneous surface of the photocatalyst, reactions (12) and (13) are two-electron production of hydrogen that controls the other reactions:



where h^+ is the positively charged hole, left after excitation of titanium dioxide. A two-electron reaction (10) of carbon dioxide to carbon monoxide occurs in the semiconductor conduction band. It could be considered an intermediate step to the eight-electron reaction (11) towards methane. Also, two-step electron and proton-assisted electron transfer to N_2 (reduction reactions (14) and (15)) occur in the same conduction band [29]:



Other multi-step reactions with lower energy transition values (between -1.10 and 0.55 V vs. NHE) additionally occurs (reactions (16)-(21)) [52]:



When considering the mechanism and competition in the above gaseous mixture, the nature of individual gases must be taken into account. Nitrogen, regardless of the reduction mechanism to ammonia (dissociative pathway or associative alternating pathway or associative distal pathway) at the time of adsorption, is an inert gas [29,44]. Then, after hydrogen bonding, it is transformed into an alkaline compound. Therefore, it locates on the acidic active sites of the photocatalyst.

On the other hand, carbon dioxide is acidic in nature. Thus, it adsorbs on alkaline active sites. For this reason, the competition between the nitrogen reduction reaction and the carbon dioxide reduction reaction indicates the superiority of the nitrogen fixation reaction. The obtained results indicate that the introduction of nitrogen to the gaseous reaction mixture significantly slows down the eight-electron reaction of methane formation and even blocks it.

Summarizing the mechanism, it can be said that in the system we deal with two reactants that compete in the reduction mechanism – CO_2 and N_2 . Probably the active sites of the reaction are distant from each other, because CO_2 , as a slightly acidic reagent, is adsorbed on reduction sites of an alkaline nature with higher adsorption potential or neutral site nature, where from nitrogen and hydrogen ammonia is formed. It can be said that separate adsorption sites for different reactants cause the reactions of CO_2 reduction and N_2 reduction to run in parallel, especially since ammonia quickly leaves the reaction environment.

The explanation for diminishing of oxidation of ammonia may come from the competition between the rapid absorption of ammonia gas in the water and the oxidation of ammonia by oxygen from water decomposition. Affinity of ammonia to liquid water is higher than ammonia to adsorption on oxidation photocatalysts sites and further oxidation on holes by pathway with oxygen coming from water decomposition.

4. Conclusions

A new method of obtaining ammonia from nitrogen gas and water vapor saturated with CO_2 at a temperature of 20 °C has been presented. In this method, an essential element is to keep the photocatalyst P25 bed just above the water surface, and the direction of gas circulation is to the water surface. Furthermore, the use of glass fibers as support of titanium dioxide nanoparticles is also positive, as the transparency of the fibers for UV radiation are expected.

In water, the produced ammonia was immediately absorbed to form

NH_4^+ ions – maximum about 1.3 mmol NH_4^+ /g TiO_2 after 6 h of the process, which causes the ammonia synthesis equilibrium to shift towards the product. In the case of the simultaneous presence of nitrogen and carbon dioxide, in addition to the ammonium ions in water, specific amounts of gas-phase reduction of CO_2 products was observed after 6 h, that was carbon monoxide (max. approx. 100 μ mol CO /g TiO_2/dm^3), small amounts of hydrogen (1 – 2 μ mol H_2 /g TiO_2/dm^3), and also methane – about 7 μ mol CH_4 /g TiO_2/dm^3 .

Raising the reaction temperature from 20 °C to 50 °C did not significantly increase the amount of ammonia produced (increased from 1.28 mmol NH_4^+ /g TiO_2 to 1.34 mmol NH_4^+ /g TiO_2 after 6 h), but eliminated the production of carbon monoxide (reduction from about 100 μ mol/g TiO_2/dm^3 to about 5 μ mol/g TiO_2/dm^3 after 6 h). In addition, no methane was observed in the processes with increased nitrogen content, regardless of the process temperature.

No competition was found between reducing nitrogen to ammonia and carbon dioxide to carbon monoxide. It can be explained by the different chemical nature of both gases. Nitrogen is inert, and carbon dioxide is acidic in nature, so the adsorption determining the activity is carried out on acidic sites for nitrogen and in alkaline places for carbon dioxide.

Moreover, the presence of carbon dioxide in a mixture with nitrogen prefers the six-electron reduction reaction of nitrogen to ammonia and, at the same time, the two-electron reduction reaction of carbon dioxide to carbon monoxide. As a result, the eight-electron reduction of carbon dioxide to methane is entirely restrained. The ammonia produced from a mixture of N_2 and CO_2 is absorbed in water and reacts to NH_4^+ ions bound to ammonium hydrogen carbonate NH_4HCO_3 or ammonium carbonate $(NH_4)_2CO_3$, except for the experiment with pure N_2 atmosphere where it appears as NH_4OH .

The presented new method of obtaining green ammonia using a unique photoreactor design with quick capture of ammonia in water, which moves reaction equilibrium to the product, is very effective because the obtained amounts of ammonia are at the millimolar level. It exceeds the literature data, which are generally at the micromolar range. The method of obtaining ammonia described in this article has been patent-pending [51].

Declaration of Competing Interest

The authors declare that they have no known competing financial interests or personal relationships that could have appeared to influence the work reported in this paper.

Acknowledgement

The research leading to these results has received funding from the Norway Grants 2014-2021 via the National Centre for Research and Development under the grant number NOR/POLNORCCS/PhotoRed/0007/2019-00.

We gratefully acknowledge the time and effort of Agnieszka Wojciechowska in taking AFM images of our materials.

Authors contributions

All authors assisted in collecting the data, the data analysis, and the preparation of the manuscript. All authors have read and agreed to the published version of the manuscript.

References

- [1] F.Y. Al-Aboosi, M.M. El-Halwagi, M. Moore, R.B. Nielsen, Renewable ammonia as an alternative fuel for the shipping industry, *Curr. Opin. Chem. Eng.* 31 (2021), 100670, <https://doi.org/10.1016/j.coche.2021.100670>.
- [2] X. Peng, F.-X. Liu, Y. Zhang, Z.-Q. Fuang, L. Yang, Y. Jiang, X. Wang, L. Zheng, C. Chang, C. Au, L. Jiang, J. Li, Highly efficient ammonia synthesis at low

- temperature over a Ru-Co catalyst with dual atomically dispersed active centers, *Chem. Sci.* 12 (2021) 7125–7137, <https://doi.org/10.1039/D1SC00304F>.
- [3] V. Kyriakou, I. Garagounis, A. Vourros, E. Vasileiou, M. Stoukides, An electrochemical Haber-Bosch process, *Joule* 4 (2020) 142–158, <https://doi.org/10.1016/j.joule.2019.10.006>.
- [4] H. Hirakawa, M. Hashimoto, Y. Shiraishi, T. Hirai, Photocatalytic conversion of nitrogen to ammonia with water on surface oxygen vacancies of titanium dioxide, *J. Am. Chem. Soc.* 139 (2017) 10929–10936, <https://doi.org/10.1021/jacs.7b06634>.
- [5] K. Nakata, A. Fujishima, TiO₂ photocatalysis: design and applications, *J. Photochem. Photobiol. C* 13 (2012) 169–189, <https://doi.org/10.1016/j.jphotochemrev.2012.06.001>.
- [6] A. Jain, D. Vaya, Photocatalytic activity of TiO₂ nanomaterial, *J. Chil. Chem. Soc.* 62 (2017) 3683–3690, <https://doi.org/10.4067/s0717-97072017000403683>.
- [7] S.A. Ansari, M.M. Khan, M.O. Ansari, M.C. Cho, Nitrogen-doped titanium dioxide (N-doped TiO₂) for visible light photocatalysis, *New J. Chem.* 40 (2016) 3000–3009, <https://doi.org/10.1039/C5NJ03478G>.
- [8] M. Peñas-Garzón, W.H.M. Abdelraheem, C. Belver, J.J. Rodriguez, J. Bedia, D. Dionysiou, TiO₂-carbon microspheres as photocatalysts for effective remediation of pharmaceuticals under simulated solar light, *Sep. Purif. Technol.* 275 (2021) 119169.
- [9] J. Prakash, S. Sun, H.C. Swart, R.K. Gupta, Noble metals-TiO₂ nanocomposites: from fundamental mechanisms to photocatalysis, surface enhanced Raman scattering and antibacterial applications, *Appl. Mater. Today* 11 (2018) 82–135, <https://doi.org/10.1016/j.apmt.2018.02.002>.
- [10] G.N. Schrauzer, T.D. Guth, Photolysis of water and photoreduction of nitrogen on titanium dioxide, *J. Am. Chem. Soc.* 99 (22) (1977) 7189–7193, <https://doi.org/10.1021/ja00464a015>.
- [11] G.N. Schrauzer, Photoreduction of nitrogen on TiO₂ and TiO₂-containing minerals, energy efficiency and renewable energy through nanotechnology, in: L. Zhang (Ed.), *Green Energy and Technology*, Springer, London, 2011, pp. 601–623.
- [12] S. Chang, X. Xu, Au nanocrystals decorated TiO₂ nanotubes for photocatalytic nitrogen fixation into ammonia, *Inorg. Chem. Front.* 7 (2020) 620–624, <https://doi.org/10.1039/C9QI01287G>.
- [13] C.h. Li, M.Z. Gu, M.M. Gao, K.N. Liu, X.Y. Zhano, N.W. Cao, J. Feng, Y.M. Ren, T. Wei, M.Y. Zhang, N-doping TiO₂ hollow microspheres with abundant oxygen vacancies for highly photocatalytic nitrogen fixation, *J. Colloid Interface Sci.* 609 (2022) 341–352, <https://doi.org/10.1016/j.jcis.2021.11.180>.
- [14] X. Li, J. Li, H. Zhai, M. Song, L. Wang, R. Guan, Q. Zhang, Z. Zhao, Efficient catalytic fixation nitrogen activity under visible light by molybdenum doped mesoporous TiO₂, *Catal. Lett.* 152 (2022) 116–123, <https://doi.org/10.1007/s10562-021-03625-5>.
- [15] W. Zhao, J. Zhang, X. Zhu, M. Zhang, J. Tang, M. Tan, Y. Wang, Enhanced nitrogen photofixation on Fe-doped TiO₂ with highly exposed (101) facets in the presence of ethanol as scavenger, *Appl. Catal. B* 144 (2014) 468–477, <https://doi.org/10.1016/j.apcatb.2013.07.047>.
- [16] B.M. Comer, A.J. Medford, Analysis of photocatalytic nitrogen fixation on rutile TiO₂ (110), *ACS Sustain. Chem. Eng.* 6 (2018) 4648–4660, <https://doi.org/10.1021/acsschemeng.7b03652>.
- [17] X.-Y. Xie, P. Xiao, W.-H. Fang, G. Cui, W. Thiel, Probing photocatalytic nitrogen reduction to ammonia with water on the rutile TiO₂ (110) surface by first-principles calculation, *ACS Catal.* 9 (2019) 9178–9187, <https://doi.org/10.1021/acscatal.9b01551>.
- [18] Q.-Y. Liu, H.-D. Wang, R. Tang, Q. Cheng, Y.-J. Yuan, Rutile TiO₂ nanoparticles with oxygen vacancy for photocatalytic nitrogen fixation, *ACS Appl. Nano Mater.* 4 (2021) 8674–8679, <https://doi.org/10.1021/acsnm.1c02184>.
- [19] S. Liu, Y. Wang, S. Wang, M. You, S. Hong, T.-S. Wu, Y.-L. Soo, Z. Zhao, G. Jiang, J. Qiu, B. Wang, Z. Sun, Photocatalytic fixation of nitrogen to ammonia by single Ru atom decorated TiO₂ nanosheets, *ACS Sustain. Chem. Eng.* 7 (2019) 6813–6820, <https://doi.org/10.1021/acsschemeng.8b06134>.
- [20] Y. Liao, J. Lin, B. Cui, G. Xie, S. Hu, Well-dispersed ultrasmall ruthenium on TiO₂(P25) for effective photocatalytic N₂ fixation in ambient condition, *J. Photochem. Photobiol. A* 387 (2020), 112100, <https://doi.org/10.1016/j.jphotochem.2019.112100>.
- [21] M. Lan, N. Zheng, X. Dong, Y. Wang, J. Wu, X. Ren, J. Gao, Application of flexible PAN/BioBr-Cl microfiber as self-supporting and highly active photocatalyst for nitrogen fixation and dye degradation, *Appl. Surf. Sci.* 575 (2022), 151743, <https://doi.org/10.1016/j.apsusc.2021.151743>.
- [22] X. Liu, Y. Luo, C. Ling, Y. Shi, G. Zhan, H. Li, H. Gu, K. Wei, F. Guo, Z. Ai, L. Zhang, Rare earth La single atoms supported MoO_{3-x} for efficient photocatalytic nitrogen fixation, *Appl. Catal. B* 301 (2022), 120766, <https://doi.org/10.1016/j.apcatb.2021.120766>.
- [23] J. Wang, Y. Fang, W. Zhang, X. Yu, L. Wang, Y. Zhang, TiO₂/BioBr 2D–2D heterostructure via in-situ approach for enhanced visible-light photocatalytic N₂ fixation, *Appl. Surf. Sci.* 567 (2021), 150623, <https://doi.org/10.1016/j.apsusc.2021.150623>.
- [24] X. Li, J. Chang, S. Zhang, L. Xiao, X. Wu, Z. He, Microcystis@TiO₂ nanoparticles for photocatalytic reduction reactions: nitrogen fixation and hydrogen evolution, *Catalysts* 11 (2021) 1443, <https://doi.org/10.3390/catal11121443>.
- [25] Y. Shen, L. Chen, L. Zhang, W. Han, M. Jiang, H. Zheng, Nitrogen fixation from air at normal temperature and pressure via cobalt-iron photocatalyst day and night, *Mol.* 518 (2022), 112091, <https://doi.org/10.1016/j.mcat.2021.112091>.
- [26] C.E. Choong, M. Park, Y.-Y. Chang, J.-K. Yang, J.R. Kim, S.-E. Oh, B.-H. Jeon, E. H. Choi, Y. Yoon, M. Jang, Interfacial coupling perovskite CeFeO₃ on layered graphitic carbon nitride as a multifunctional Z-scheme photocatalyst for boosting nitrogen fixation and organic pollutants demineralization, *Chem. Eng. J.* 427 (2022), 131406, <https://doi.org/10.1016/j.cej.2021.131406>.
- [27] X. Bian, Y. Zhao, S. Zhang, D. Li, R. Shi, Ch. Zhou, L.-Z. Wu, T. Zhang, Enhancing the supply of activated hydrogen to promote photocatalytic nitrogen fixation, *ACS Mater. Lett.* 3 (2021) 1521–1527, <https://doi.org/10.1021/acsmaterialslett.1c00504>.
- [28] R. Li, Photocatalytic nitrogen fixation: an attractive approach for artificial photocatalysis, *Chinese J. Catal.* 39 (2018) 1180–1188, [https://doi.org/10.1016/S1872-2067\(18\)63104-3](https://doi.org/10.1016/S1872-2067(18)63104-3).
- [29] Z. Wang, J. Hong, S.-F. Ng, W. Liu, J. Huang, P. Chen, W.-J. Ong, 2021. Recent progress of perovskite oxide in emerging photocatalysis landscape: water splitting, CO₂ reduction, and N₂ fixation. *Acta Phys. – Chim. Sin.* 37(6), 2011033. <https://doi.org/10.3866/PKU.WHXB202011033>.
- [30] S. Zhang, Y. Zhao, R. Shi, G.I.N. Waterhouse, T. Zhang, Photocatalytic ammonia synthesis: recent progress and future, *Energy. Chem.* 1 (2) (2019) 100013.
- [31] D. Pan, Z. Han, Y. Miao, D. Zhang, G. Li, Thermally stable TiO₂ quantum dots embedded in SiO₂ foams: characterization and photocatalytic activity, *Appl. Catal. B: Environ.* 229 (2018) 130–138, <https://doi.org/10.1016/j.apcatb.2018.02.022>.
- [32] J. Fernandez-Catala, D. Cazorla-Amoros, A. Berrenguer-Murcia, Facile encapsulation of P25 (TiO₂) in spherical silica with hierarchical porosity with enhanced photocatalytic properties for gas-phase propene oxidation, *Appl. Catal. A Gen.* 564 (2018) 123–132, <https://doi.org/10.1016/j.apcata.2018.07.024>.
- [33] E. Pakdel, W.A. Daoud, S. Seyedin, J. Wang, J.M. Razal, L. Sun, X. Wang, Tunable photocatalytic selectivity of TiO₂/SiO₂ nanocomposites: Effect of silica and isolation approach, *Colloids Surf. A Physicochem. Eng. Asp.* 552 (2018) 130–141, <https://doi.org/10.1016/j.colsurfa.2018.04.070>.
- [34] O.K. Park, Y.S. Kang, Preparation and characterization of silica-coated TiO₂ nanoparticle, *Colloids Surf. A Physicochem. Eng. Asp.* 257–258 (2005) 261–265, <https://doi.org/10.1016/j.colsurfa.2004.10.014>.
- [35] J. Kapica-Kozar, E. Piróg, R.J. Wróbel, S. Mozia, E. Kusiak-Nejman, A. W. Morawski, U. Narkiewicz, B. Michalkiewicz, TiO₂/titanate composite nanorod obtained from various alkali solutions as CO₂ sorbents from exhaust gases, *Microporous and Mesoporous Mater.* 231 (2016) 117–127, <https://doi.org/10.1016/j.micromeso.2016.05.024>.
- [36] M. Janus, E. Kusiak-Nejman, A.W. Morawski, Determination of the photocatalytic activity of TiO₂ with high adsorption capacity, *React. Kinet. Mech. Catal.* 103 (2011) 279–288, <https://doi.org/10.1007/s11444-011-0326-z>.
- [37] Actinic BL TL-E 22W/10 1CT/20. <https://www.lighting.philips.com/main/prof/conventional-lamps-and-tubes/special-lamps/insect-trap/actinic-bl/actinic-bl-tl-e/928026201005EU/product> (accessed 04 January 2022).
- [38] R. Fuang, X. Li, W. Gao, X. Zhang, S. Liang, M. Luo, Recent advances in photocatalytic nitrogen fixation: from active sites to ammonia quantification methods, *RSC Adv.* 11 (2021) 14844–14861, <https://doi.org/10.1039/d0ra10439f>.
- [39] A.W. Morawski, K. Ćmiełowska, K. Witkowski, E. Kusiak-Nejman, I. Pelech, P. Staciwa, E. Ekiert, D. Sibera, A. Wanag, M. Gano, U. Narkiewicz, CO₂ reduction to valuable chemicals on TiO₂-carbon photocatalysts deposited on silica cloth, *Catalysts* 12 (2022) 31, <https://doi.org/10.3390/catal12010031>.
- [40] E. Kusiak-Nejman, A. Czyżewski, A. Wanag, M. Dubick, M. Sadiowski, R.J. Wróbel, A.W. Morawski, Photocatalytic oxidation of nitric oxide over AgNPs/TiO₂-loaded carbon fiber cloths, *J. Environ. Manag.* 262 (2020), 110343, <https://doi.org/10.1016/j.envman.2020.110343>.
- [41] P. Murzyn, G. Malata, J. Wiśniewska, E. Kapeluszná, W. Nocuń-Wzelik, Characterization of 40-year-old calcium silicate pastes by thermal methods and other techniques, *J. Therm. Anal. Calorim.* 138 (2019) 4271–4278, <https://doi.org/10.1007/s10973-019-08519-8>.
- [42] G. Chen, J. Chen, Z. Song, C. Srinivasakannan, J. Peng, A new highly efficient method for the synthesis of rutile TiO₂, *J. Alloys Compd.* 585 (2014) 75–77, <https://doi.org/10.1016/j.jallcom.2013.09.056>.
- [43] W.M. Shaheen, K.S. Hong, Thermal characterization and physico-chemical properties of Fe₂O₃Mn₂O₃/Al₂O₃ systems, *J. Therm. Anal. Cal.* 68 (2002) 289–306, [https://doi.org/10.1016/S0040-6031\(01\)00652-9](https://doi.org/10.1016/S0040-6031(01)00652-9).
- [44] W. Ren, Z. Mei, S. Zheng, S. Li, Y. Zhu, J. Zheng, Y. Lin, H. Chen, M. Gu, F. Pan, Wavelength-dependent solar N₂ fixation into ammonia and nitrate in pure water, *Research* (2020) 3750314, <https://doi.org/10.34133/2020/3750314>.
- [45] M.J. Mitchell, O.E. Jensen, K.A. Cliffe, M.M. Maroto-Valer, A model of carbon dioxide dissolution and mineral carbonation kinetics, *Proc. Math. Phys. Eng. Sci.* 466 (2010) 1265–1290, <https://doi.org/10.1098/rspa.2009.0349>.
- [46] K. Saruhashi, On the equilibrium concentration ratio of carbonic acid substances dissolved in natural water. a study on the metabolism in natural waters (II), *Pap. Meteorol. Geophys.* 6 (1955) 38–55. <https://doi.org/10.2467/mripapers1950.6.1.38>.
- [47] P.W.J. Derks, G.F. Vestee, Kinetics of absorption of carbon dioxide in aqueous ammonia, *Energy Procedia* 1 (2009) 1139–1146, <https://doi.org/10.1016/j.egypro.2009.01.150>.
- [48] J. Liu, S. Wang, B. Zhao, H. Tong, C. Chen, Absorption of carbon dioxide in aqueous ammonia, *Energy Procedia* 1 (2009) 933–940, <https://doi.org/10.1016/j.egypro.2009.01.124>.
- [49] P. Wang, G. Yin, Q. Bi, X. Huang, X. Du, W. Zhao, F. Huang, Efficient photocatalytic reduction of CO₂ using carbon-doped amorphous titanium oxide, *Chem. Cat. Chem.* 10 (2018) 3854–3861, <https://doi.org/10.1002/cctc.201800476>.
- [50] M. Tasbihi, K. Koci, I. Troppova, M. Edelmanna, M. Reli, L. Capek, R. Schömacker, Photocatalytic reduction of carbon dioxide over Cu/TiO₂

- photocatalysts, *Environ. Sci. Pollut. Res.* 25 (2018) 34903–34911, <https://doi.org/10.1007/s11356-017-0944-8>.
- [51] A.W. Morawski, U. Narkiewicz, K. Ćmielewska, E. Kusiak-Nejman, I. Pelech, P. Staciwa, E. Ekiert, D. Sibera, A. Wanag, M. Gano, Ammonia production method and ammonia production reactor (Sposób wytwarzania amoniaku i reaktor do wytwarzania amoniaku), Polish Patent Application, P.439745 (06.12.2021).
- [52] H. Shen, M. Yang, L. Hao, J. Wang, J. Strunk, Z. Sun, Photocatalytic nitrogen reduction to ammonia: insights into the role of defect engineering in photocatalysts, *Nano Res.* 15 (2022) 2773–2809, <https://doi.org/10.1007/s12274-021-3725-0>.